BMC Genomics

RESEARCH

Open Access

Evaluating the mouse neural precursor line, SN4741, as a suitable proxy for midbrain dopaminergic neurons

Rachel J. Boyd[1†], Sarah A. McClymont[1†], Nelson B. Barrientos[1], Paul W. Hook[1], William D. Law[1], Rebecca J. Rose[1], Eric L. Waite[1], Jay Rathinavelu[1], Dimitrios Avramopoulos[1] and Andrew S. McCallion[1,2*]

Abstract

To overcome the ethical and technical limitations of in vivo human disease models, the broader scientific community frequently employs model organism-derived cell lines to investigate disease mechanisms, pathways, and therapeutic strategies. Despite the widespread use of certain in vitro models, many still lack contemporary genomic analysis supporting their use as a proxy for the affected human cells and tissues. Consequently, it is imperative to determine how accurately and effectively any proposed biological surrogate may reflect the biological processes it is assumed to model. One such cellular surrogate of human disease is the established mouse neural precursor cell line, SN4741, which has been used to elucidate mechanisms of neurotoxicity in Parkinson disease for over 25 years. Here, we are using a combination of classic and contemporary genomic techniques – karyotyping, RT-qPCR, single cell RNA-seq, bulk RNA-seq, and ATAC-seq – to characterize the transcriptional landscape, chromatin landscape, and genomic architecture of this cell line, and evaluate its suitability as a proxy for midbrain dopaminergic neurons in the study of Parkinson disease. We find that SN4741 cells possess an unstable triploidy and consistently exhibits low expression of dopaminergic neuron markers across assays, even when the cell line is shifted to the non-permissive temperature that drives differentiation. The transcriptional signatures of SN4741 cells suggest that they are maintained in an undifferentiated state at the permissive temperature and differentiate into immature neurons at the non-permissive temperature; however, they may not be dopaminergic neuron precursors, as previously suggested. Additionally, the chromatin landscapes of SN4741 cells, in both the differentiated and undifferentiated states, are not concordant with the open chromatin profiles of ex vivo, mouse E15.5 forebrain- or midbrain-derived dopaminergic neurons. Overall, our data suggest that SN4741 cells may reflect early aspects of neuronal differentiation but are likely not a suitable proxy for dopaminergic neurons as previously thought. The implications of this study extend broadly, illuminating the need for robust biological and genomic rationale underpinning the use of in vitro models of molecular processes.

Keywords Parkinson disease, Mouse-derived cell lines, Immortalized cell lines, Chromatin accessibility, RNA-seq, ATAC-seq, scRNA-seq, Genomic characterization, Disease-relevant model systems

†Rachel J. Boyd and Sarah A. McClymont contributed equally to this work.

*Correspondence:
Andrew S. McCallion
andy@jhmi.edu
Full list of author information is available at the end of the article

Background

In vitro cellular surrogates present an excellent opportunity for elucidating the molecular mechanisms behind human disease without the ethical and technical limitations of in vivo systems. As such, most studies of human disease that employ genomic or cellular manipulations or assays that require high cell quantity and quality, are often conducted in vitro to ensure biological and statistical robustness [1–3]. For example, in vitro models are frequently employed in studies of the role of genomic regulation in human disease, identification of candidate genes and regulatory elements and evaluation of their functional characteristics through genetic manipulations and high-throughput assays [4–7]. As genome-wide association studies (GWASs) continue to reveal human disease-associated variants, it is becoming evident that most of them lie within non-coding regions of the genome [8]. Such regions frequently represent cis-regulatory elements (CREs), required for the transcriptional modulation of cognate genes. The assays required to evaluate their function [4, 9, 10], or connect CREs with the promoters they modulate [11], often require large cell numbers, making, in vitro cellular systems the preferred strategy.

Prioritizing non-coding GWAS variants and disease-relevant sequences for extensive investigation requires knowledge of their chromatin accessibility status. Open chromatin is prone to harbor functional sequences; and since chromatin accessibility profiles vary across cell types and developmental time, it is important to prioritize disease-associated variants that lie within open chromatin regions in the disease-relevant cell type(s) [8, 12, 13]. It is also critical to functionally evaluate the biological consequences of disease-associated variation, test the efficacy of potential therapeutics, and observe the effects of disease-relevant insults in the appropriate cellular context [8, 14, 15]. Therefore, when studying disease associated variation, the most effective in vitro cellular surrogates should ideally mimic the chromatin architecture and transcriptional profiles of the in vivo cell types affected by disease.

In Parkinson disease (PD), midbrain (MB) dopaminergic (DA) neurons in the substantia nigra (SN) are the primary affected cell type [16]. Preferential degeneration of these neurons elicits a progressive neurodegenerative disorder characterized by motor deficits [16]. As the second most common neurodegenerative disorder, affecting approximately 1% of adults over 70 years old [17, 18], PD is the focus of extensive research efforts. As such, various cell lines have been used as in vitro proxies of MB DA neurons to study the cellular impacts of PD-relevant insults, as well as candidate PD-associated sequences, their functions, and their potential as therapeutic targets [19].

One such cell line, SN4741, is reported to be a clonal DA neuronal progenitor line that was established in 1999 from mouse embryonic day 13.5 (E13.5) SN tissue [20]. The SN was dissected from transgenic mice containing 9.0 kb of the 5' promoter region of rat tyrosine hydroxylase (*Th*), fused to the temperature-sensitive mutant Simian Virus 40 T antigen (SV40Tag-tsA58) oncogene [20]. The goal of this *Th* promoter transgene was to enable selective acquisition of DA neurons, while the purpose of the SV40Tag oncogene was to facilitate conditional immortalization of the cell line. The temperature sensitive mutant form of this immortalizing gene (tsA58) should permit uncontrolled differentiation and proliferation at the permissive temperature (33 °C), maintain cells in an undifferentiated state at 37 °C, and since tsA58 displays diminished activity at 39 °C, it should direct differentiation that more closely resembles primary cells when the culture is shifted to this non-permissive temperature [20].

As an established mouse neural precursor line, SN4741 cells have since been used to elucidate mechanisms of neurotoxicity in PD [21–25], test the efficacy of therapeutic targets against PD relevant insults [26, 27], and assay the impacts of PD-associated genetic mutation [28, 29] and transcriptional regulation [30–32]. Important technological advances have also arisen since the genesis and implementation of the SN4741 cell line, including chromatin conformation capture technologies [11, 33, 34], RNA-sequencing (RNA-seq) [35], and assay for transposase-accessible chromatin using sequencing (ATAC-seq) [36]. In this study, we exploit these modern approaches to assess the suitability of SN4741 as an in vitro proxy for DA neurons and determine the extent to which this cell line is appropriate for prioritizing and investigating the mechanisms by which PD-associated variation confers disease risk.

Through a combination of karyotyping, single-cell (sc)RNA-seq, and RT-qPCR, we evaluate the genomic integrity of this immortalized cell line, determine how the transcriptional profile and expression of DA neuron marker genes in this line changes between undifferentiated (37 °C) and differentiated (39 °C) states, and evaluate whether these transcriptional changes are consistent throughout the differentiation process. The data we collect suggests that while these cells show evidence that they are exiting a proliferative state and entering a more differentiated state, they are an unsuitable model of SN DA neurons, as they possess aneuploidy and structural abnormalities, as well as consistently low expression of DA neuron markers upon differentiation. We employ bulk RNA-seq to quantify transcriptional differences

between differentiated and undifferentiated SN4741 cells and determine that, while transcriptional profiles change to reflect differentiation, they do not show strong evidence that these cells are entering a DA state. We then compare chromatin accessibility profiles of undifferentiated and differentiated SN4741 cells with those of ex vivo mouse E15.5 midbrain (MB) and forebrain (FB) neurons and determine that the chromatin accessibility profiles of SN4741 cells do not reflect the cellular population from which they were derived. Collectively, cytogenetic, chromatin, and transcriptional data suggest that the SN4741 cell line is not as strong a cellular surrogate for DA neurons as previously thought. Ultimately, this work underscores the importance of leveraging technological advances in genomic and cellular analyses to evaluate, and re-evaluate, the suitability of established model systems in disease biology.

Results

SN4741 is an unstable polyploid cell line

G-band karyotyping was performed on 20 SN4741 metaphase spreads and a representative karyogram (Fig. 1A) was generated. The karyotype was interpreted as an abnormal, polyploid, karyotype with complex numerical

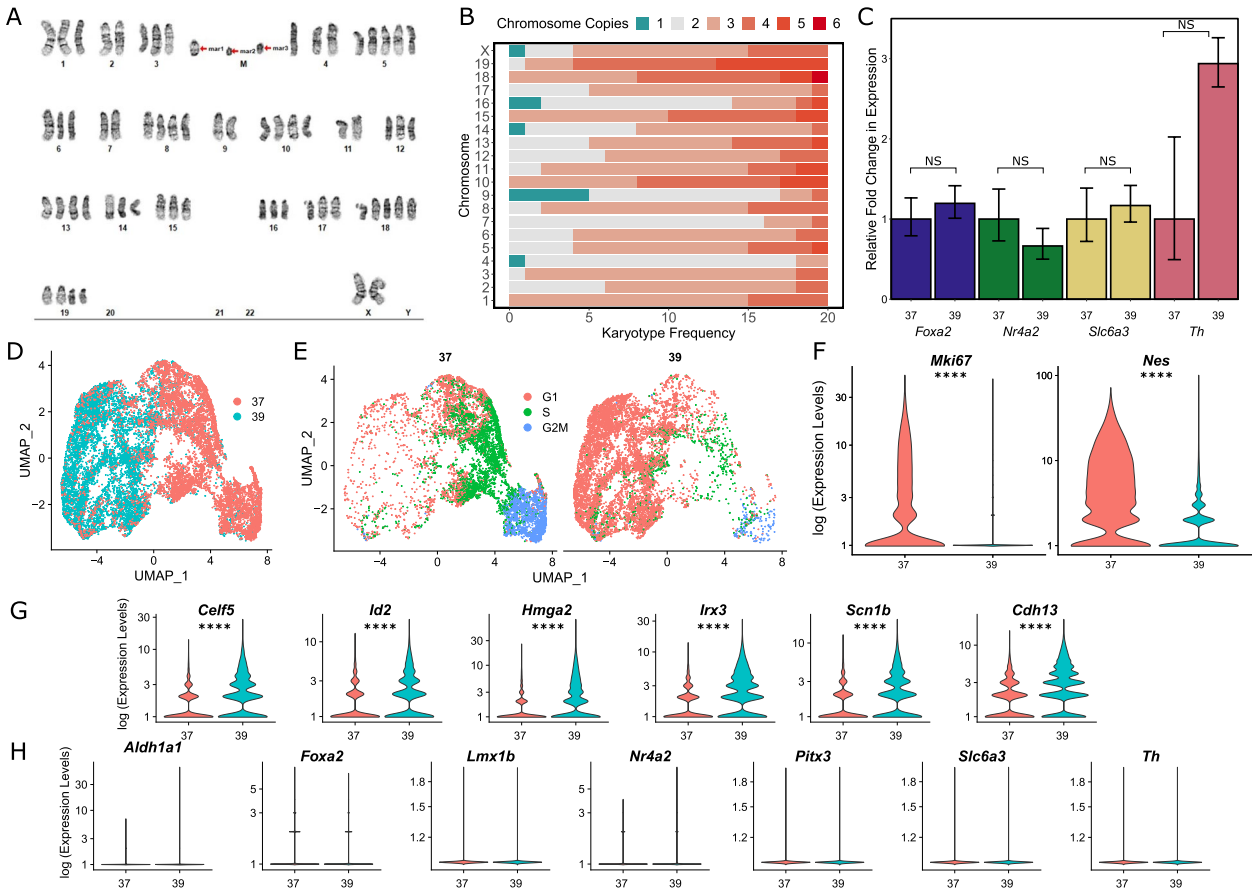

Fig. 1 Characterizing the genomic stability and differentiation consistency of the temperature sensitive SN4741 cell line. **A** A representative karyogram of SN4741 cells, indicating structural instability (M; marker chromosomes) and unstable triploidy. **B** A stacked bar plot summarizing the aneuploidy frequency of each chromosome over 20 SN4741 karyotypes. **C** Assaying expression of dopaminergic neuron markers by RT-qPCR indicates that *Foxa2*, *Nr4a2*,*Slc6a3*, and *Th* remain at similar expression levels when SN4741 cells are shifted from the permissive temperature (37 °C) to the non-permissive temperature (39 °C). **D** UMAP plot of scRNA-seq at the permissive and non-permissive temperatures indicates that cells at each temperature are transcriptionally distinct. **E** Analysis of scRNA-seq data demonstrates that shifting the cells to the non-permissive temperature is accompanied by a shift in cell cycle stage from G2M and S phases to primarily G1 phase. **F** Violin plots generated with scRNA-seq data show that *Mki67*, a marker of cellular proliferation, and *Nes*, a neural stem cell marker, are both expressed at the permissive temperature (37 °C), with little to no expression at the non-permissive temperature (39 °C). **G** Violin plots generated with scRNA-seq data show that transcripts associated with immature neurons are upregulated when SN4741 cells are shifted to the non-permissive temperature. **H** Violin plots generated with scRNA-seq data show that expression of DA neural markers, *Aldh1a1*, *Foxa2*, *Lmx1b*, *Nr4a2*, *Pitx3*, *Slc6a3*, and *Th*, remain at similar levels when SN4741 cells are shifted to the non-permissive temperature. (NS = Not significant, * = $p < 0.05$, ** = $p < 0.01$, *** = $p < 0.001$, **** = $p < 0.0001$)

abnormalities and unbalanced, structural abnormalities. While most, but not all, abnormalities were consistently present in these cells; none of the 20 cells assessed had the same chromosome complement, and no normal cells were observed. All cells possessed at least one copy of each mouse autosome (1 through 19) and female sex chromosomes; however, most chromosomes were triploid in each cell (Fig. 1B). These karyotypic abnormalities already call into question the viability of these cells as a surrogate for human neurodegenerative disease. Since these cells are genetically unstable, there may be large experimental batch effects as the cell populations shift across divisions. Furthermore, gene dosage effects that severely deviate from normal copy number in DA neurons may lead to confounding and unreliable results.

Undifferentiated and differentiated SN4741 cells express similar levels of dopaminergic neuron marker genes by RT-qPCR

Preliminary analysis by RT-qPCR confirmed expression of a variety of DA neuron markers: forkhead box A2 (*Foxa2*), nuclear receptor subfamily 4 group A, member 2 (*Nr4a2*), solute carrier family 6 member 3 (*Slc6a3*), and tyrosine hydroxylase (*Th*). Compared to the expression of these markers in the undifferentiated SN4741 cell culture (37 °C), relative expression of all markers remained at similar levels (*Foxa2*, $p = 0.601$; *Nr4a2*, $p = 0.425$; *Slc6a3*, $p = 0.729$; *Th*, $p = 0.265$) when the cells were shifted to the higher temperature condition (39 °C), (Fig. 1C). While elevated *Th* has been used as a marker of differentiation into DA neurons in previous work with SN4741 cells [20, 37, 38], an increase in *Th* expression is not exclusively associated with DA neurons. *Th* is a marker for all catecholaminergic neurons (dopaminergic and adrenergic) [39], and evidence suggests that *Th* expression is transient in other neurons throughout embryonic development [40–42]. These results indicate that at the non-permissive temperature, SN4741 cells may not be fully differentiating into DA neuron progenitors.

scRNA-seq reveals that SN4741 cells differentiate at the non-permissive temperature, but lack expression of DA neuron marker genes

To assess the consistency of the differentiation protocol, transcriptomes were generated from ≥ 17,000 cells across four replicates cultured at the permissive temperature (37 °C) and four replicates cultured at the non-permissive temperature (39 °C). Analysis of the single-cell transcriptomes reveal that the cells cluster by growth temperature (Fig. 1D). This separation of cells by temperature is accompanied by changes to the cell cycle, with cells at the permissive (37 °C) temperature mostly in either G2M or S phase, while cells at the non-permissive temperature (39 °C) are mostly in G1 phase (Fig. 1E), indicating that they may be differentiated. In expression analysis, markers of proliferation that are expressed in G2M phase, like Marker of Proliferation Ki-67 (*Mki67*), are predominantly expressed in cells at the permissive temperature ($p < 2.225\text{e-}308$, Fig. 1F), corroborating the cell cycle analysis. When shifted to the non-permissive temperature, SN4741 cells appear to robustly differentiate, exemplified by a decrease in the expression of Nestin (*Nes*), a neural stem cell marker ($p < 2.225\text{e-}308$, Fig. 1F). Additional transcriptional changes at this non-permissive temperature include a significant increase in the expression of a neural marker CUGBP Elav-Like Family Member 5 (*Celf5*, $p < 2.225\text{e-}308$) [43], as well as genes that have been found to regulate neural stem cell self-renewal (Inhibitor of DNA Binding 2, *Id2*, $p = 9.236\text{e-}251$; High Mobility Group AT-Hook 2, *Hmga2*, $p < 2.225\text{e-}308$) [44, 45], neurogenesis (Iroquois Homeobox 3, *Irx3*, $p < 2.225\text{e-}308$) [46], and arborization of neurons (Sodium Voltage-Gated Channel Beta Subunit 1, *Scn1b*, $p < 2.225\text{e-}308$) [47], indicating that these cells may be differentiating into neural precursor cells (Fig. 1G). Furthermore, Cadherin 13 (*Cdh13*, $p < 2.225\text{e-}308$), a modulator of GABAergic neurons, is significantly upregulated at this non-permissive temperature (Fig. 1G), while the expression of a variety of DA neuron markers, including Aldehyde Dehydrogenase 1 Family Member A1 (*Aldh1a1*), *Foxa2*, LIM Homeobox Transcription Factor 1 Beta (*Lmx1b*), *Nr4a2*, Paired-like homeodomain 3 (*Pitx3*), *Slc6a3*, and *Th*, fail to meet the criteria differential expression analysis (Fig. 1H). Collectively, these results suggest that while SN4741 cells are differentiating towards a neuronal fate when shifted to the nonpermissive temperature, they may not be entering a clear DA trajectory under these conditions.

ATAC-seq identifies differential open chromatin profiles in SN4741 cells at the permissive and non-permissive temperatures

To consider how chromatin accessibility changes between the two temperatures, we performed ATAC-seq on SN4741 cells in both the undifferentiated and differentiated states. Libraries were confirmed to be technically and biologically relevant (Supplemental Fig. 1), and well correlated between replicates (Supplemental Fig. 2; Fig. 2A-B).

A total of 83,778 consensus open chromatin regions were identified, with 70% of peaks shared between the two temperatures (Fig. 2C). Principal component analysis of these consensus regions suggests a clear separation in the chromatin state between the two temperatures (Fig. 2D). To explore these differences, we performed differential accessibility analysis with DiffBind [48], to

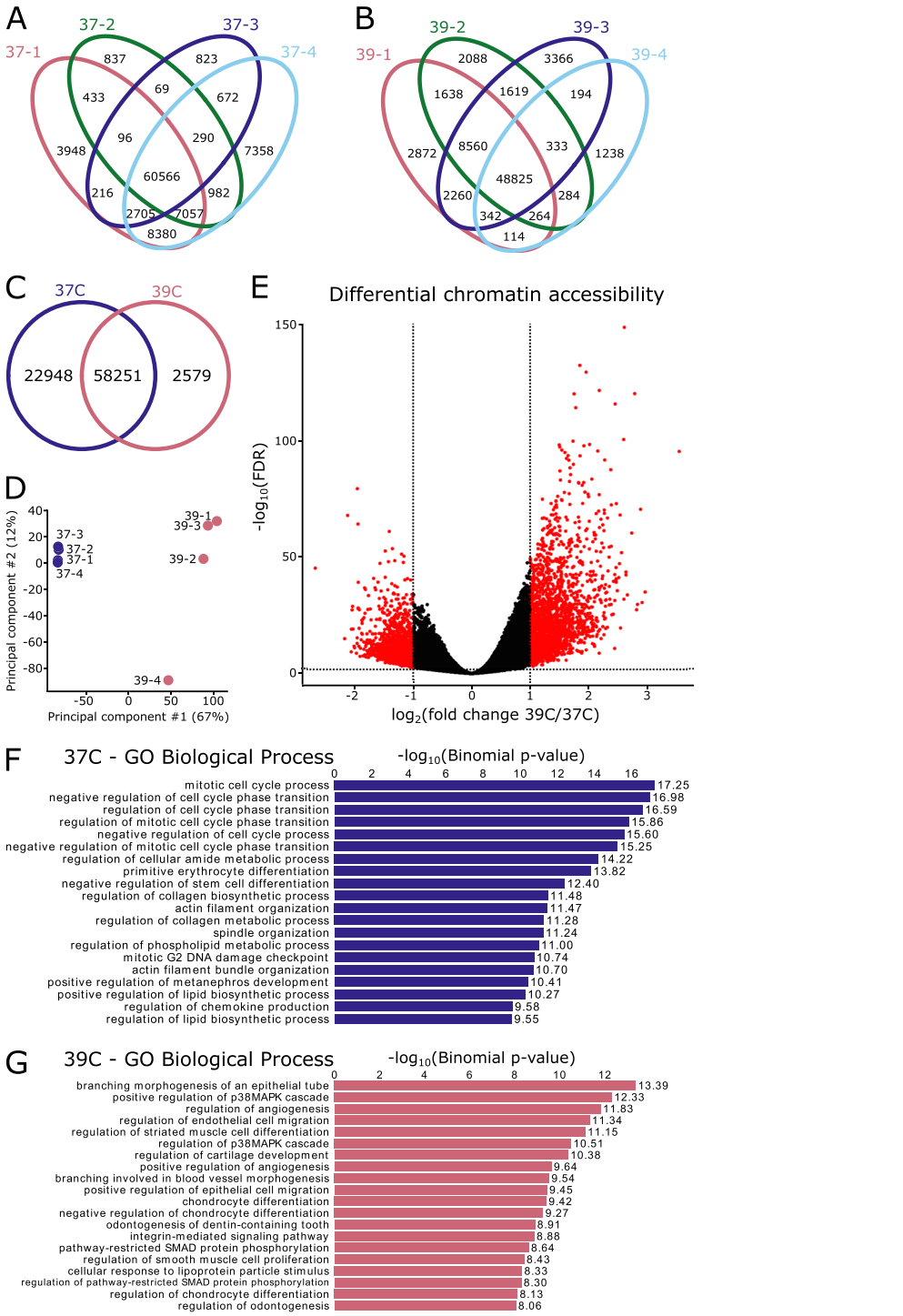

Fig. 2 Changes in chromatin accessibility suggest a reduction in potency at the non-permissive temperature. **A**, **B** Replicates are highly similar within temperature conditions, with the majority of peaks present in all four replicates. **C** The two temperatures share 58,251 regions of open chromatin but do not overlap completely. **D** Principal component analysis resolves the two temperatures on the first principal component. **E** Differential accessibility analysis identifies 5,055 differentially accessible regions, with 2,654 preferentially open in the permissive temperature (37 °C) and 2,401 preferentially accessible at the non-permissive temperature (39 °C). **F** Gene ontology (GO) of genes adjacent regions that are preferentially open at the permissive temperature are associated with regulation of the cell cycle and negative regulation of differentiation, as is appropriate for this temperature. **G** Gene ontology of genes adjacent regions that are preferentially open at the non-permissive temperature are associated with a variety of differentiation fates (blood vessels, muscle cells, cartilage/chondrocytes). Additionally, two of the top gene ontology terms relate to the p38 MAPK cascade, which has been found to be activated as a cellular response to heat stress

find a total of 5,055 differentially accessible regions: 2,654 enriched in the permissive temperature and 2,401 enriched at the non-permissive temperature ($\log_2$FC > 1, FDR < 0.05; Fig. 2E).

Gene ontology of genes adjacent to differentially accessible regions largely recapitulate the scRNA-seq analysis; functions associated with regions preferentially open at the permissive temperature suggest the maintenance of the undifferentiated, cell-cycling state (Fig. 2F). The gene ontology of genes adjacent to those regions preferentially accessible at the non-permissive temperature is less coherent and suggest cell differentiation towards several fates (blood vessels, cartilage, tooth), none of which are neuronal and, perhaps unsurprisingly, demonstrate evidence of response to temperature stress [49] (Fig. 2G).

Overall, there is a shift in the chromatin accessibility between the two temperatures that indicates that the cells transition from an undifferentiated to differentiated state as the cells move from the permissive to non-permissive temperature. The differences in chromatin accessibility further confirm that SN4741 cells are not differentiating towards a neuronal lineage.

Comparison of chromatin accessibility in SN4741 cells fails to recapitulate the chromatin landscape of ex vivo mouse DA neurons

To evaluate the potential relationship between SN4741 cells and DA neurons they are presumably modelling, we compared the chromatin accessibility between the SN4741 cells at both temperatures to previously generated ex vivo mouse embryonic DA neuron chromatin accessibility profiles (NCBI GEO: GSE122450; [50]).

Considering the consensus peak set of 165,334 regions generated from all in vivo and ex vivo samples and their normalized read counts, we observe a clear separation between the SN4741 cell culture model and the ex vivo DA neurons by correlation and principal component analysis (Fig. 3A, B). Examining the raw overlap of peaks between the SN4741 cells and ex vivo neurons, just 12.5% (20,667) are present in all four cell types/conditions (Fig. 3C). The chromatin profiles are largely exclusive between the SN4741 cell culture model and the ex vivo DA neurons: 41.3% (68,304) of regions are accessible solely in the ex vivo neuron populations and 40% (65,857) are exclusively accessible in the SN4741 cell culture models. There is little overlap between the ex vivo and cultured samples. In comparison of the ex vivo midbrain DA neurons to the non-permissive, differentiated temperature, only 183 peaks are restricted to these populations.

The chromatin profiles between ex vivo embryonic DA neurons and their prospective in vitro cell culture surrogate are virtually independent. They exhibit scant overlap in their global chromatin profiles and bear little resemblance to each other at regulatory regions of key DA neuron genes (Fig. 3D). It is worth noting that the lack of concordant data between in vivo SN4741 cells (2D culture) and ex vivo DA neurons (3D) may also be due, in part, to differences in culturing and isolation conditions. Previous studies have found that 2D culture conditions do not fully recapitulate in vivo or ex vivo 3D conditions [51, 52]. Regardless, neither the analysis of the SN4741 chromatin accessibility profiles in isolation or in comparison with ex vivo neurons would suggest these cells to be appropriate models of embryonic DA neurons.

Transcriptional changes in SN4741 cells indicate differentiation from pluripotent stem cells into brain cells that do not fully resemble MB DA neurons

Bulk RNA-seq data were also generated for SN4741 cells, at both the permissive and non-permissive temperatures, to determine whether transcriptome changes reflect differentiation into DA neurons, or other neural cell types. To evaluate the RNA-seq libraries, quality-control measures were performed in silico (Supplemental Fig. 3). PCA (Supplemental Fig. 3B), and sample-sample distances (Supplemental Fig. 3C) reaffirmed that samples cultured at the same temperature are more like one-another than samples cultured at the alternate temperature.

We found that 735 genes were upregulated at the non-permissive temperature (adjusted p-value < 0.01 and $\log_2$ FC > 1.5), and 954 genes were downregulated (adjusted p-value < 0.01 and $\log_2$ FC < -1.5) at the non-permissive temperature. The list of genes significantly downregulated at the non-permissive temperature was submitted to Enrichr (https://maayanlab.cloud/Enrichr/) [53–55] for gene ontology (GO) and analysis of cell type markers. Consistent with the observation that cells at the non-permissive temperature are differentiated and in G1 phase of the cell cycle, downregulated genes resulted in GO terms strongly enriched for mitotic and DNA replication processes (Fig. 4A). Additionally, significantly downregulated genes at the non-permissive temperature overlap with subsets of PanglaoDB [56] cell type marker genes, suggesting that these cells are shifting away from a state that resembles neural stem cells (Fig. 4B).

Similarly, the list of significantly upregulated genes was submitted to Enrichr for GO and analysis of cell type markers. As expected, upregulated genes resulted in GO terms for biological processes that indicate a more terminally differentiated cell type (Fig. 4C): "synaptic vesicle docking", "negative regulation of osteoblast proliferation", "lens fiber cell differentiation", "regulation of osteoblast proliferation", and "forebrain regionalization". While not included in the top 10 terms by combined score ranking, "neuron remodeling", "synaptic transmission, glutamatergic", "neuron maturation", and "synaptic transmission,

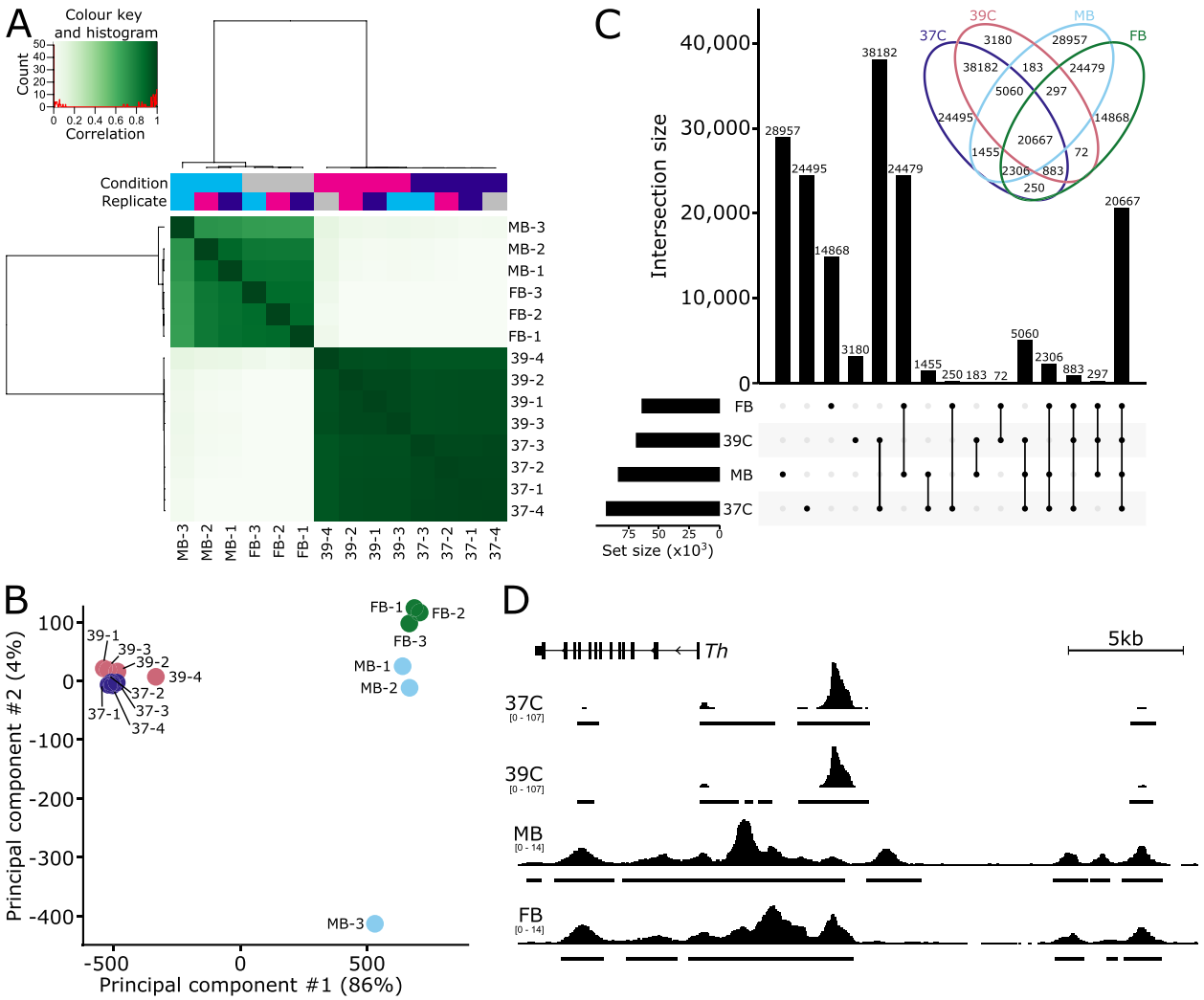

Fig. 3 Chromatin accessibility of SN4741 cells do not resemble ex vivo dopaminergic neurons. **A** SN4741 samples are highly correlated with each other but very poorly correlate with the open chromatin landscape of either midbrain (MB) or forebrain (FB) embryonic mouse dopaminergic neurons. **B** Principal component analysis shows a clear separation between the ex vivo and in vitro samples along PC1, representing 86% of the variance. **C** An upset plot and associated Venn diagram quantify the overlap of peaks between the four conditions and show the poor relationship between the SN4741 cells and the ex vivo mouse dopaminergic neurons. Most peaks are specific to a single cell type/temperature or are restricted to either the ex vivo or in vitro samples. Few peaks are specifically shared between the non-permissive temperature and the ex vivo samples; for example, there are just 183 peaks that are shared exclusively by the MB dopaminergic neurons and the SN4741 cells at the non-permissive temperature. **D** A genome track showing the normalized read pile up and called consensus peaks in each of the cell types/temperatures at the key dopaminergic neuron specification gene, *Th*. The chromatin accessibility is largely similar within ex vivo or in vitro cells but bear little resemblance to each other

cholinergic" were also identified as significantly associated terms. Notably, "synaptic transmission, dopaminergic" and "dopaminergic neuron differentiation" were also listed as insignificant terms (Fig. 4C), as *Th* was the lone overlapping marker gene for these terms.

In line with GO terms enriched for biological processes involving differentiation, possibly in neuronal cells, overlapping PanglaoDB [56] cell type marker genes suggest that SN4741 cells at the non-permissive temperature most significantly resemble immature neurons (Fig. 4D). "Oligodendrocytes", "retinal progenitor cells", "satellite glial cells", "dopaminergic neurons", "adrenergic neurons", "GABAergic neurons", and "glutamatergic neurons" were also listed as cell types with significant marker gene overlap.

The distribution of various cell type marker genes on a volcano plot, indicating the $\log_2$FC in expression and $-\log_{10}$ adjusted *p*-values of DE genes, reveals that the

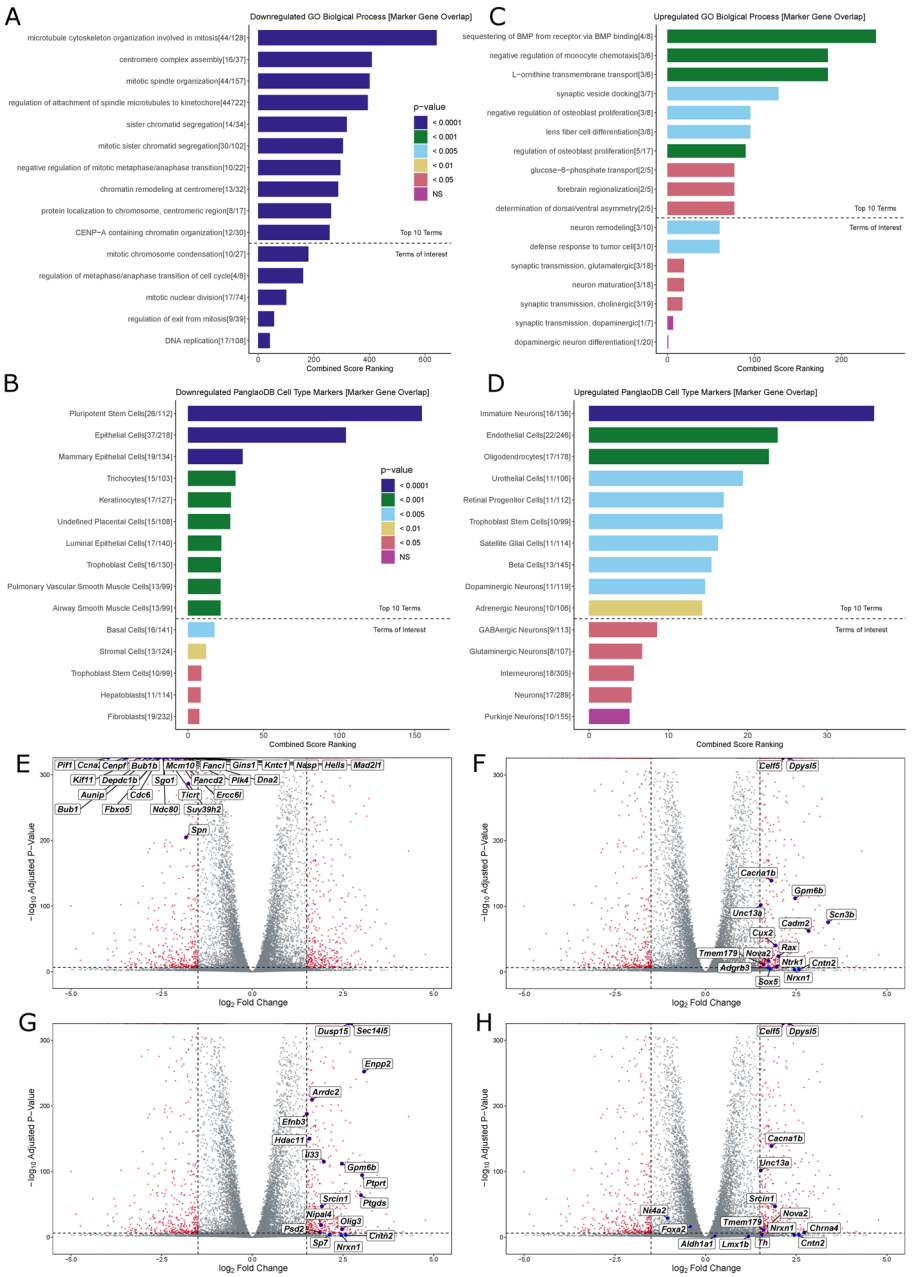

Fig. 4 Gene Ontology and Differential Expression Analysis of Bulk RNA-seq Data: **A** Top 10 GO terms for downregulated DE genes in SN4741 cells at the non-permissive temperature, followed by GO terms of interest (below dotted line). Terms were evaluated using Combined Score Ranking = (*p*-value computed using the Fisher exact test)*(z-score computed by assessing the deviation from the expected rank), based on enrichment of DE genes that overlap with Enrichr input genes for each term (the end of each bar). **B** Top 10 predicted cell types based on downregulated DE genes in SN4741 cells at the non-permissive temperature, followed by predicted cell types of interest (below dotted line). Terms were evaluated using Combined Score Ranking = (*p*-value computed using the Fisher exact test)*(z-score computed by assessing the deviation from the expected rank), based on enrichment of DE genes that overlap with PanglaoDB input genes for each term (the end of each bar). **C** Top 10 GO terms for downregulated DE genes in SN4741 cells at the non-permissive temperature. **D** Top 10 predicted cell types based on upregulated DE genes in SN4741 cells at the non-permissive temperature. **E** Volcano plot of –log10 adjusted *p*-value versus $\log_2$ fold change with DESeq2 after lfc shrinkage, contrasting the fold change in expression of SN4741 cells at 39 °C, using SN4741 cells at 37 °C as reference. Red points = genes that are statistically differentially expressed (adjusted *p*-value < 0.01, $|\log_2 FC| > 1.5$). Blue points = Overlapping immature neuron marker genes. **F** Blue points = Overlapping immature neuron marker genes. **G** Blue points = Overlapping oligodendrocyte marker genes. **H** Blue points = Overlapping DA neuron marker genes

specific genes overlapping "pluripotent stem cell" markers (26/112), cluster as the most highly significantly downregulated genes (Fig. 4E). In contrast, only two of the upregulated marker genes overlapping "immature neurons" (16/136, Fig. 4F) and "oligodendrocytes" (17/178, Fig. 4G) cluster in a similarly strong way. Plotting the 11/119 overlapping upregulated genes for "dopaminergic neurons" (Fig. 4H) reveals that 7/11 overlapping genes (*Celf5*, *Dpys15*, *Cacna1b*, *Tmem179*, *Nova2*, *Nrx1*, and *Cntn2*) are also marker genes for immature neurons. Plotting the DA neuron markers also assayed by RT-qPCR validates that the relative expression of these markers is consistent between these highly sensitive assays. At 39 °C, *Th* expression significantly increases ($log_2FC = 1.552651$, $p = 3.779e\text{-}05$); *Nr4a2* ($log_2FC = -1.042794$, $p = 1.555e\text{-}30$) and *Foxa2* ($log_2FC = -0.4142541$, $p = 1.303e\text{-}17$) expression actually decreases, but does not meet the thresholds set for differential expression due to a low fold-change in expression; and *Slc6a3* was filtered out due to low read counts across both temperature conditions.

To confirm the GO-indicted cell types, normalized read counts for select marker genes were plotted for each temperature replicate: *Celf5* ($p < 2.225e\text{-}308$) [43], *Nrxn1* ($p = 0.0002$) [57], *Ntrk1* ($p = 4.907e\text{-}09$) [58], and *Unc13a* ($p = 1.719e\text{-}103$) [59], for "immature neurons" were upregulated at 39 °C relative to cells at 37 °C (Fig. 5A); *Olig3* ($p = 1.101e\text{-}13$) [60], *Il33* ($p = 6.241e\text{-}117$) [61], *Hdac11* ($p = 3.778e\text{-}152$) [62], and *Ptgds* ($p = 8.108e\text{-}66$) [63] for "oligodendrocytes" were upregulated at 39 °C relative to cells at 37 °C (Fig. 5B); and *Ccna2* ($p < 2.225e\text{-}308$) [64], *Cdc6* ($p < 2.225e\text{-}308$) [65], *Cenpf* ($p < 2.225e\text{-}308$) [66], and *Gins1* ($p < 2.225e\text{-}308$) [67] for "pluripotent stem cells" were downregulated at 39 °C relative to cells at 37 °C (Fig. 5C).

The differentially expressed gene sets were then analyzed using STRING (https://string-db.org/) [68]. The set of upregulated genes was enriched for protein-protein interactions (number of edges = 705; expected number of edges = 438; PPI enrichment *p*-value = < 1.0e-16) and GO terms such as "Neuron differentiation" (GO:0030182; FDR = 0.0016), "Neuron development" (GO:0048666; FDR = 0.0070), and "Neurogenesis" (GO:0022008; FDR = 0.0085) supporting that this upregulated gene set is a meaningful group likely belonging to a network involved in neuronal maturation. The set of downregulated genes was also enriched for protein-protein interactions (number of edges = 9251; expected number of edges = 1910; PPI enrichment *p*-value = < 1.0e-16) and GO terms such as "Cell cycle" (GO:0007049; FDR = 5.90e-36), "Mitotic cell cycle" (GO:0000278; FDR = 6.97e-34), and "Cell division" (GO:0051301; 6.35e-25) further confirming that these cells are no longer undergoing cell division.

Finally, previously generated reads per kilobase of exon per million reads mapped (RPKM) from ex vivo E15.5 mouse embryonic DA neuron bulk RNA-seq [50] were used to compare how closely the SN4741 transcriptome resembles the neuronal populations they are expected to model. Similar to our results comparing chromatin accessibility between these two datasets, correlation of RPKM shows a clear separation between the SN4741 cell culture model and the ex vivo DA neurons (average r^2: MB vs 37 = 0.653; MB vs 39 = 0.659; FB vs 37 = 0.636; FB vs 39 = 0.643) (Fig. 5D). Collectively, these results confirm that at the non-permissive temperature, SN4741 cells are no longer rapidly dividing neural stem cells. However, while the transcriptional profile of these cells indicates that they are differentiating towards cell types present in the brain, these cells do not fully possess characteristics of the MB DA neurons they are meant to model.

Discussion

It is critically important that studies of human disease generate biologically accurate data, whether aimed at elucidating molecular mechanisms, onset and progression, or management and therapeutics. In the context of discovery biology or the illumination of human health and disease mechanisms, misattribution of cellular identity, or other deviations from biological accuracy, may result the misinterpretation of biological findings or misdirected research efforts. When studying human disease, cellular surrogates are often used to overcome the ethical and technical limitations of employing animal models. Therefore, it is imperative that disease-relevant insights are predicated on robust data generated from model systems representing human biology as accurately as possible.

Here, we demonstrate the importance of assessing in vitro models of disease to determine the extent to which they can yield biologically accurate data that can be used to inform aspects of human disease. The SN4741 cell line has been used to study neurotoxicity and therapeutic interventions [21–27], PD-associated genetic mutation [28, 29] and cell signaling and transcriptional regulation [30–32, 37], since it was initially characterized as an immortal, mouse MB-derived cell line that differentiates into DA neurons at a non-permissive temperature [20]. However, contemporary genomic analyses have not been leveraged to characterize and evaluate the SN4741 cell line as a suitable proxy for DA neurons in PD, until now.

We employed karyotyping, RT-qPCR, and scRNA-seq to assess the genomic stability of these cells and determine how consistently they differentiate into DA neurons at the non-permissive temperature. We generated bulk RNA-seq and ATAC-seq data from this cell line at

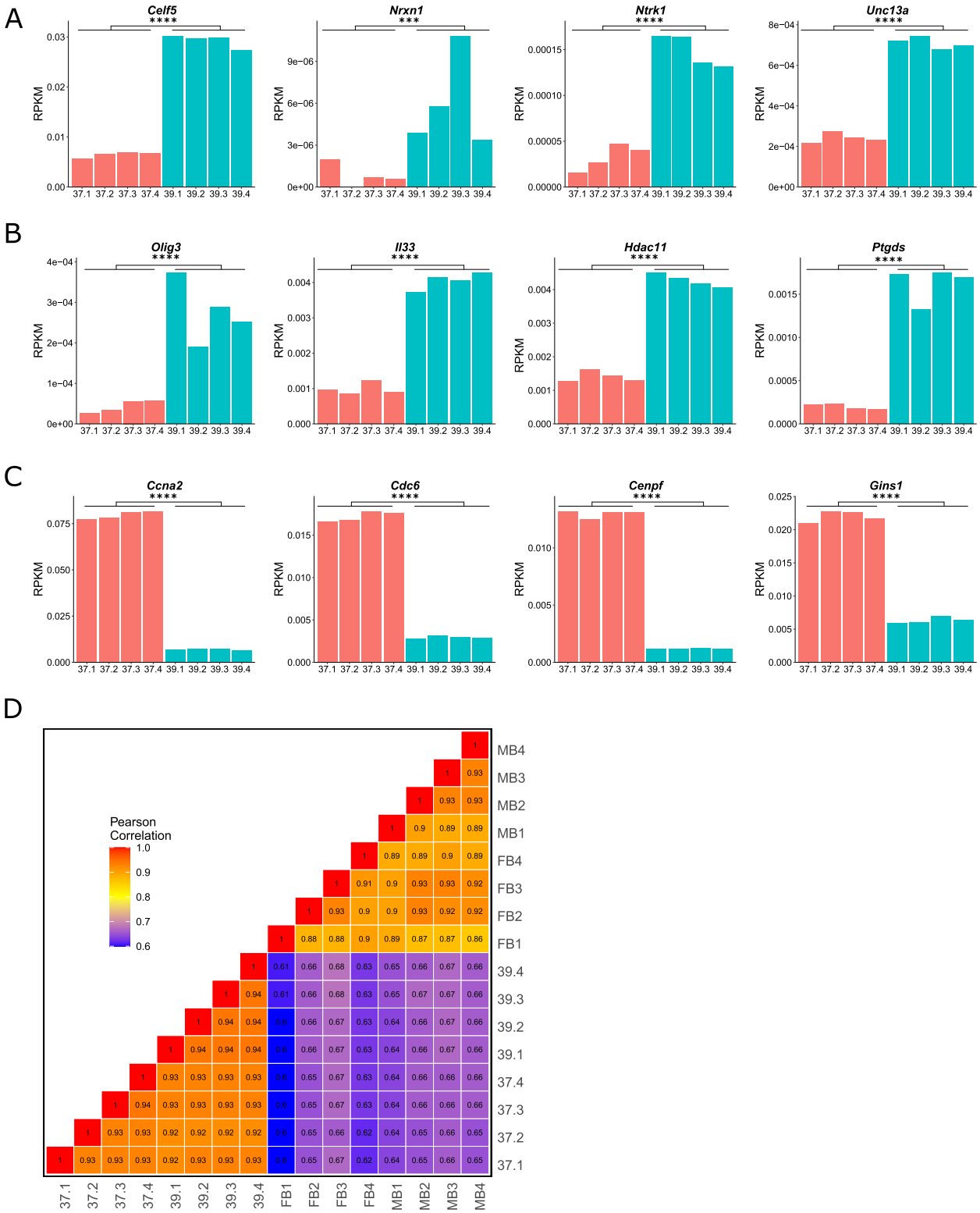

Fig. 5 Validation of gene ontology and comparison to bulk-RNA-seq from ex vivo DA neurons. **A** A bar chart showing normalized bulk RNA-seq read counts from genes upregulated at 39 °C that overlap the "immature neurons" predicted cell type. **B** A bar chart showing normalized bulk RNA-seq read counts from genes upregulated at 39 °C that overlap the "oligodendrocyte" predicted cell type. **C** A bar chart showing normalized bulk RNA-seq read counts from genes downregulated at 39 °C that overlap the "pluripotent stem cell" predicted cell type. **D** A Pearson correlation heatmap comparing the transcriptomes of SN4741 cells at 37 °C and 39 °C to midbrain (MB) or forebrain (FB) embryonic mouse dopaminergic neurons. (NS = Not significant, * = $p < 0.05$, ** = $p < 0.01$, *** = $p < 0.001$, **** = $p < 0.0001$)

both the permissive and non-permissive temperatures, to extensively characterize this cell line and document how transcriptional landscapes and chromatin accessibility profiles shift in response to temperature-induced differentiation and compare to known profiles of ex vivo DA neurons. Our results suggest that SN4741 is an unstable, polyploid cell line that is unlikely to be a viable differentiation model of DA neurons; and thus, is likely not a robust proxy by which to study MB DA neurons in the context of human phenotypes, including PD, schizophrenia, addiction, memory, or movement disorders.

The results of karyotyping alone indicate that any data generated using SN4741 cells may be biologically inaccurate due to extreme variability in chromosome complement and therefore, copy number variation, between individual cells. Consequently, the results of previous studies evaluating neurotoxicity [21, 23, 24, 26, 27, 30, 32, 38], cellular signaling pathways [22, 25, 28, 69, 70], and transcriptional profiling [37] in these cells may have been unduly influenced by the extreme imbalance in gene dosage that we found to vary from cell to cell. For example, alpha-synuclein (*SNCA*) has been consistently implicated in PD risk [71–74], particularly due to variants that promote α-synuclein misfolding [75] and overexpression [50] or events that result in gene amplification [76, 77]. *Snca* is present on mouse chromosome 6 and the karyotypes generated for SN4741 cells show that chromosome 6 is triploid in most assayed cells (Fig. 1B). Therefore, using the SN4741 cell line to model neurodegeneration in PD may result in inaccurate data due to an exaggerated vulnerability towards degeneration imposed by elevated *Snca* copy number, by gene dosage effects of other interacting gene products in relevant pathways, or by the structural instability of this line.

Even if this cell line could be adopted to study *Snca* overexpression/amplification, ATAC-seq profiling of open chromatin regions in this cell line at the permissive and non-permissive temperatures indicates that these cells do not possess chromatin accessibility profiles similar to those of ex vivo, mouse E15.5 MB neurons. In PD, disease is characterized by the degeneration of MB DA neurons, while DA neurons of the FB are spared. Therefore, the chromatin profiles of MB DA neurons, as well as the differentially accessible regions of the genome between MB and FB neurons, may influence the preferential vulnerability of MB neurons in PD [50]. In the context of exploiting these chromatin profiles to study PD-associated variability and neurotoxicity, SN4741 cells are likely a poor model, as the open chromatin regions of these cells are not a reliable proxy for mouse E15.5 MB or FB DA neurons.

The chromatin accessibility profiles of SN4741 cells not only fail to cluster with ex vivo populations of mouse MB neurons, but the transcriptional landscapes of these cells suggest that these cells have shifted towards a more differentiated state that may be less DA than previously thought. Examination of cell cycle markers by scRNA-seq demonstrates that SN4741 cells at the non-permissive temperature are more differentiated than cells at the permissive temperature, as expected [20]. GO terms for genes that are significantly downregulated at the non-permissive temperature reinforces that these cells are no longer rapidly dividing, pluripotent stem cells. However, RT-qPCR, scRNA-seq, and bulk RNA-seq in these cells fail to detect significant upregulation of most key DA neuron markers in the differentiated cells, except for *Th* in the bulk RNA-seq data. *Th* is not exclusively expressed by DA neurons at embryonic timepoints [40–42]. In fact, significantly upregulated genes in SN4741 cells at the non-permissive temperature that overlap with GO terms and cell cycle marker genes suggests that *Th* is the only significantly upregulated gene overlapping with biological processes involving DA neurons. Rather, additional overlapping cell type marker genes suggest that these cells more closely resemble immature neurons.

In parallel, we generated promoter capture (pc)Hi-C data at the non-permissive temperature with the intention of exploring how non-coding disease-relevant variants interact with promoters and potentially regulate gene expression in MD DA neurons. As our group is focused on PD-associated variation, which is unlikely to act broadly in immature neurons, our group has not analyzed the resulting data, beyond basic quality control (Supplemental Fig. 4). While the SN4741 cells at the non-permissive temperature fail to recapitulate the transcriptomic or chromatin state of DA neurons, it is of potential interest for follow-up studies that they do resemble some immature neuron types. Although not analyzed by our group, we generated output files for interaction detection, and this data has been made publicly available for others to explore (accessible through: https://github.com/rachelboyd/SN4741_pcHiC), as it may be useful to study genomic interactions at promoters driving an immature neuronal state. However, the cell type best represented by SN4741 cells at the non-permissive temperature still requires deeper characterization.

Any data generated using SN4741 cells in the context of DA neuron modeling and/or PD must be interpreted with caution and in light of the appropriate caveats. Due to the instability and polyploidy of this cell line, we recommend that the use of SN4741 cells for PD- related research be re-evaluated. Future studies designed to fine-tune the classification of these cells may support the use of SN4741 cells as a model of other neuronal or non-neuronal cells. Additionally, the differentiation trajectory of these cells may be amenable to intervention(s) that could

drive their molecular state towards one that resembles DA neurons more closely.

Conclusions

This study establishes a valuable precedent with broad implications across biological and disease-related research. Prior to using SN4741 cells to study non-coding regulatory variation in PD, we characterized this cell line to determine its suitability as a model of DA neurons in PD, and found that these cells are unstable, polyploid cells that do not demonstrate strong molecular characteristics of MB DA neurons. These cells express low levels of DA neuron markers, and chromatin landscapes in differentiated SN4741 cells scarcely overlap open chromatin regions in ex vivo mouse E15.5 midbrain neurons. We demonstrate the importance of genomic characterization of in vitro model systems prior to generating data and valuable resources that may be used to inform aspects of human disease. In future studies that utilize in vitro models of any human disease, due diligence to confirm their suitability as surrogates could save time, resources, and possibly lives, by avoiding misdirection and advancing successful therapeutic development.

Methods

No animals were directly used in this study. All assays were carried out using animal-derived cell lines or publicly available animal-derived cell data.

Cell culture

SN4741 cells were obtained from the Ernest Arenas group at the Karolinska Institutet. SN4741 cells were confirmed to be mycoplasma free using a MycoAlert® Mycoplasma Detection Assay (Lonza) and were maintained in high glucose Dulbecco's Modified Eagle Medium (DMEM; Gibco 1196502), supplemented with 1% penicillin–streptomycin and 10% fetal bovine serum (FBS) in a humidified 5% CO_2 incubator at 37 °C. Cells at 80% confluence were passaged by trypsinization approximately every 2–3 days. To induce differentiation, 24 h after the cells were passaged, media was replaced by DMEM supplemented with 1% penicillin–streptomycin and 0.5% FBS at 39 °C. Cells were allowed to grow and differentiate in these conditions for 48 h before harvesting for experimentation.

G-band karyotyping

At passage 21, undifferentiated SN4741 cells were sent to the WiCell Research Institute (Madison, Wisconsin), at 40–60% confluency, for chromosomal G-band analyses. Karyotyping was conducted on 20 metaphase spreads, at a band resolution of > 230, according to the International System for Human Cytogenetic Nomenclature.

cDNA synthesis and RT-qPCR for DA neuron markers

RNA was extracted from both differentiated and undifferentiated cells by following the RNeasy Mini Kit (QIAGEN) protocol, as written. Extracted RNA was quantified using a Nanodrop. 1 µg of each RNA sample underwent first-strand cDNA synthesis using the SuperScript III First-Strand Synthesis System for RT-PCR (Invitrogen) according to the oligo(dT) method. qPCR was performed with Power SYBR Green Master Mix (Applied Biosystems), using primers for β-actin (*Actb*), *Foxa2*, *Nr4a2*, *Slc6a3*, and *Th* (Table S1). Reactions were run in triplicate under default SYBR Green Standard cycle specifications on the Viia7 Real-Time PCR System (Applied Biosystems). Normalized relative quantification and error propagation followed the data analysis and associated calculations proposed by Taylor et al. (2019) [78], with results normalized to *Actb* and a t-test was performed using R function "t.test", (alternative = "two.sided"). The remaining RNA and cDNA were subsequently stored at -80 °C.

Single cell RNA-seq library preparation, sequencing, and alignment

Both differentiated (39 °C) and undifferentiated (37 °C) cells were trypsinized, and scRNA-seq libraries were generated following the Chromium 10X pipeline [79]. Four replicates at each temperature across > 17,000 cells were assayed. Cell capture, cDNA generation, and library preparation were performed with the standard protocol for the Chromium Single Cell 3' V3 reagent kit. Libraries were quantified with the Qubit dsDNA High Sensitivity Assay (Invitrogen) in combination with the High Sensitivity DNA Assay (Agilent) on the Agilent 2100 Bioanalyzer. Single-cell RNA-sequencing libraries were pooled and sequenced on an Illumina NovaSeq 6000 (SP flow cells), using 2 × 50 bp reads per library, to a combined depth of 1.6 billion reads. The quality of sequencing was evaluated via FastQC. Paired-end reads were aligned to the mouse reference genome (mm10) using the CellRanger v3.0.1 pipeline. Unique molecular identifier (UMI) counts were quantified per gene per cell ("cellranger count") and aggregated ("cellranger aggr") across samples with no normalization.

Single cell RNA-seq analysis

Using Seurat [80] (v4.2.0), cells were filtered to remove stressed/dying cells (% of reads mapping to the mitochondria > 15%) and empty droplets or doublets (number of unique genes detected < 200 or > 6,000). Cells were scored for their stage in the cell cycle using "CellCycleScoring()" on cell cycle genes provided by Seurat ("cc.genes"). Cells were then normalized using "SCTransform" (vst.flavor = "v2") and corrected for percent

mitochondrial reads and sequence depth. Principal component (PC) analysis was performed and a PC cut-off was identified using "ElbowPlot()." Using this PC cutoff and a minimum distance of 0.001, UMAP clustering was used for dimensionality reduction. Expression was plotted on a log scale with "VlnPlot()" for a variety of proliferation and DA neuron markers. Differentially expressed genes were identified using "FindMarkers" (min.diff.pct = 0.2).

ATAC-seq library preparation and quantification

ATAC-seq libraries were generated for four replicates of undifferentiated (37 °C) and differentiated (39 °C) SN4741 cells, according to the Omni-ATAC protocol [81], with minor modifications. Aliquots of 50,000 cells were centrifuged at 2000 × g for 20 min at 4 °C, and the resulting pellets were resuspended in 50µL of resuspension buffer. Cells were left to lyse for 3 min on ice before being centrifuged again at 2000 × g for 20 min at 4 °C. The resulting nuclei pellets were then tagmented, as written, using 50µL of transposition mixture and then incubated at 37 °C for 30 min in a 1000 RPM thermomixer. After transposition, DNA was purified with the Zymo DNA Clean and Concentrator -5 Kit and eluted in 21µL of elution buffer.

Pre-amplification of the transposed fragments was performed according to the conditions outlined in the Omni-ATAC protocol [81]; however, 12 pre-amplification cycles were run in lieu of qPCR amplification to determine additional cycles. The amplified libraries were prepared according to the Nextera DNA Library Prep Protocol Guide, except that libraries were purified with 40.5µL AMPure XP beads (Beckman Coulter), and 27.5µL of resuspension buffer was added to each sample. All libraries were quantified with the Qubit dsDNA High Sensitivity Assay (Invitrogen) in combination with the High Sensitivity DNA Assay (Agilent) on the Agilent 2100 Bioanalyzer.

ATAC-seq sequencing, alignment, and peak calling

Libraries were sequenced on Illumina NovaSeq 6000 (SP flow cells), using 2 × 50 bp reads per library, to a total combined depth of 1.6 billion reads. The quality of sequencing was evaluated with FastQC (v0.11.9) [82] and summarized with MultiQC (v1.13) [83]. Reads were aligned to the mouse reference genome (mm10) in local mode with Bowtie2 [84] (v2.4.1), using –X 1000 to specify an increased pair distance to 1000 bp. Samtools (v1.15.1) [85] and Picard (v2.26.11; http://broadinstitute.github.io/picard/) were used to sort, deduplicate and index reads. Peaks were called with MACS3 (v3.0.0a7; https://github.com/macs3-project/MACS) [86] and specifying --nomodel and --nolambda for the 'callpeaks()' command. Peaks overlapping mm10 blacklisted/block listed regions called by ENCODE [87, 88] and in the original ATAC-seq paper [36] were also removed with BEDTools (v2.30.0) [89].

For visualization with IGV, IGVTools (v2.15.2) was used to convert read pileups to TDFs. The fraction of reads in peaks was calculated with DeepTools (v3.5.1) [90] using the plotEnrichment command. The average mapping distance flag was extracted from the SAM files with a custom script available at our GitHub repo (https://github.com/sarahmcclymont/SN4741_ATAC/) to generate the fragment length plot. Mouse (mm10) transcriptional start site (TSS) coordinates were downloaded from the UCSC Genome Browser [91] (Mouse genome; mm10 assembly; Genes and Gene Predictions; RefSeq Genes track using the table refGene), and DeepTools (v3.5.1) [90] was used to plot the pileup of reads overtop of these TSSs. Conservation under peaks (phastCons) [92] and the genomic distribution of peaks were calculated using the Cis-regulatory Element Annotation System (CEAS) [93] and conservation tool of the Cistrome [94] pipeline. Analysis can be found at http://cistrome.org/ap/u/smcclymont/h/sn4741-atac-seq-ceas-and-conservation.

ATAC-seq normalization and differential peak analysis

Each sample's peak file and BAMs were read into and analysed with DiffBind (v3.8.1) [48]. Peaks present in two or more libraries were considered in the consensus peakset. Reads overlapping these consensus peaks were counted with 'dba.count()' specifying summits = 100, bRemoveDuplicates = TRUE. These read counts were normalized with 'dba.normalize()' on the full library size using the RLE normalization method as it is native to the DESeq2 analysis we employed in the following 'dba.analyze()' step. The volcano plot was generated using a custom script using the output of the 'dba.report()' command, where th = 1 and fold = 0 and bCounts = T, to output all peaks regardless of their foldchange or significance. Significantly differentially accessible regions (filtered for abs(Fold) > 1 & FDR < 0.05) were submitted to GREAT (v4.0.4) [95] and the gene ontology of the nearest gene, as identified with the basal + extension method (where proximal was considered to be ± 5 kb) was assessed and plotted.

ATAC-seq comparison to ex vivo MB and FB DA neurons

Previously generated ATAC-seq libraries from ex vivo E15.5 mouse embryonic DA neurons [50] were re-analyzed in parallel, following all the above alignment and filtering steps. DiffBind (v3.8.1) was used to compare the samples, as above, and the R package UpSetR (v1.4.0) [96] was used to plot the overlap of peaks between conditions.

Bulk RNA-seq library preparation, sequencing, and alignment

Cells were run through QIAshredder (Qiagen) and total RNA was extracted using the RNeasy Mini Kit (Qiagen) according to the manufacturer's recommendations, except that RNA was eluted twice in 50μL of water. Total RNA integrity was determined with the RNA Pico Kit (Agilent) on the Agilent 2100 Bioanalyzer. RNA samples were sent to the Johns Hopkins University Genetic Resources Core Facility (GRCF) for library prep (NEBNext Ultra II directional library prep kit with poly-A selection) and sequencing. The libraries were pooled and sequenced on an Illumina NovaSeq 6000 (SP flow cells), using 2×50 bp reads per library, to a combined depth of 1.6 billion reads. The quality of sequencing was evaluated via FastQC. FASTQ files were aligned to the mouse reference genome (mm10) with HISAT2 [97] (v2.0.5) and sample reads from different lanes were merged using samtools [85] (v.1.10) function "merge". Aligned reads from individual samples were quantified against the mm10 reference transcriptome with the subread [98–100] (v1.6.1) function "featureCounts" [101], using -t exon and -g gene_id (Supplemental Fig. 3A).

Bulk RNA-seq analysis

The DESeq2 (v3.15) package was used for data quality assessment and analyses. A DESeqDataSet of count data was generated using "DESeqDataSetFromMatrix" (design = ~temp). The data underwent variance stabilizing transformation (vst) prior to using "plotPCA" to visualize experimental covariates/batch effects (Supplemental Fig. 3B) and R package "pheatmap" (v1.0.12; https://CRAN.R-project.org/package=pheatmap) to visualize the sample-to-sample distances (Supplemental Fig. 3C).

Genes with an average of at least 1 read for each sample were analyzed to identify differentially expressed (DE) genes between temperature conditions, using the function "DESeq". *P*-value distribution after differential expression (DE) analysis (Supplemental Fig. 3D) verified that the majority of called DE genes are significant. Results (alpha = 0.01) were generated and subjected to log fold change shrinkage using the function "lfcShrink" (type = "apeglm") [102] for subsequent visualization and ranking. The function "plotMA" was used to generate MA plots, both before and after LFC shrinkage, to visualize the $\log_2$ fold changes attributable to the non-permissive temperature shift over the mean of normalized counts for all the samples in the DESeqDataSet (Supplemental Fig. 3E-F). MA plots demonstrated that log fold change shrinkage of the data successfully diminished the effect size of lowly expressed transcripts with relatively high levels of variability.

Volcano plots were generated using a custom function to visualize $\log_2$ fold changes of specific genes in the dataset. A gene was considered significantly differentially expressed if it demonstrated an adjusted p-value < 0.01 and $|\log_2 FC| > 1.5$. These significantly differentially expressed genes were submitted to Enrichr [53–55] for analyses within the "ontologies" and "cell types" categories. The upregulated and downregulated gene sets were passed to STRING [68] for analysis of protein-protein interactions and network relationships.

Bulk RNA-seq comparison to ex vivo MB and FB DA neurons

Read counts from the SN4741 bulk RNA-seq dataset were converted to RPKM and compared to bulk RNA-seq data from previously generated ex vivo mouse embryonic DA neurons (NCBI GEO: GSE122450; [50]). A Pearson correlation heatmap was generated using ggplot2 [103].

Promoter capture HiC library generation

PcHiC was performed as previously described [104], with minor modifications. Briefly, SN4741 cells were cultured at the non-permissive temperature and plated at five million cells per 10 cm dish. The cells were crosslinked using 1% formaldehyde, snap frozen using liquid nitrogen, and stored at -80 °C. The cells were dounce homogenized and restriction enzyme digestion, using 400 units *HindIII-HF* overnight at 37 °C. The total volume was maintained at 500μL, through addition of 1X NEBuffer 2.1. Heat inactivation was performed at 80 °C for 20 min, and biotinylated-dCTP was used for biotin fill-in reaction. Blunt-end ligation was performed using Thermo T4 DNA ligase, with cohesive end units maintained at 15,000 and buffer and water volumes adjusted to ensure a total volume of 665μL was added to each Hi-C tube. Cross-linking was performed overnight, with additional (50μL) proteinase K added for 2 h the following day. DNA purification was split across two reactions using 2 mL PhaseLock tubes, and volumes were adjusted accordingly. Each PhaseLock reaction was split again into two vials for ethanol purification, and centrifugation at step 6.3.8 was performed at room temperature. The pellets were dissolved in 450μL 1X TLE and transferred to a 0.5 mL 30kD Amicon Column. After washing, the column was inverted into a new container, and no additional liquid was added to raise the volume to 100μL. All four reactions were combined, the total volume determined, and RNAseA (1 mg/mL) equal to 1% of the total volume was added for 30 min at 37 °C.

The libraries were assessed for successful blunt-end ligation by a ClaI restriction enzyme digest of PCR products, as previously described [104]. Biotin was removed from un-ligated ends and DNA was sheared to a size of 200-300 bp using the Covaris M220 (High setting, 35 cycles of 30 s "on" and 90 s "off"; vortexing/spinning down samples and changing sonicator water every 5 cycles). Size selection was performed using AMpure XP magnetic beads, as previously described [104] except that all resuspension steps were increased by 5µL, so that 5µL could be used for QC with the High Sensitivity DNA Assay (Agilent) on the Agilent 2100 Bioanalyzer (at three stages: post-sonication, post-0.8×size-selection, and post-1.1×size-selection). The remaining protocol was performed as described. Capture probes (Arbor Biosciences; https://github.com/nbbarrientos/SN4741_pcHiC) were designed against mouse (mm10) RefSeq transcription start sites, filtering out "XM" and "XR" annotated genes. The remaining promoters were intersected with the in silico digested *HindIII* mouse genome, to retain all *HindIII* fragments containing a promoter. Potential probes sites were assessed ± 330 bp of the *HindIII* cut site on either end of the fragment and finalized probe sets were filtered using no repeats and "strict" criteria, as defined by Arbor Biosciences. After generating a uniquely indexed HiC library with complete Illumina adapters, probes targeting promoter containing fragments were hybridized following Arbor Biosciences capture protocol (v4) at 65 °C, 1 µg DNA, and one round of capture. The library was PCR amplified before sequencing on an Illumina NovaSeq 6000 (SP flow cells), using 2×50 bp reads per library, to a combined depth of 1.6 billion reads.

Promoter capture HiC data analysis

Raw pcHiC reads for each replicate ($n=4$) were evaluated for quality via FastQC. FASTQ files were mapped to mm10 using Bowtie2 [84] (v.2.4.1) and filtered using HiCUP [105] (v. 0.8). The HiCUP pipeline was configured with the following parameters: FASTQ format (Format: Sanger), maximum di-tag length (Longest: 700), minimum di-tag length (shortest: 50), and filtering and alignment statistics were reported (Supplemental Fig. 4A-C). BAM files were generated for each replicate using samtools [85] (v.1.10). DeepTools [90] (v.3.5.1) before read coverage similarities and replicate correlation was assessed using the function "multiBamSummary" (in *bins* mode) to analyze the entire genome. A Pearson correlation heatmap was generated using the function "plotCorrelation" (Supplemental Fig. 4D). As a result of high Pearson correlation coefficient among replicates ($r>0.93$), library replicates were combined. The CHiCAGO [106] (v. 1.18.0) pipeline was used to convert the merged BAM file into CHiCAGO format. The digested mm10 reference genome was used to generate a restriction map file, a baited restriction map file, and the rest of required input files (.npb,.nbpb, and.poe) required to run the CHiCAGO pipeline.

Abbreviations

ActB	β-Actin
Aldh1a1	Aldehyde Dehydrogenase 1 Family Member A1
ATAC-seq	Assay for Transposase-Accessible Chromatin using Sequencing
BAM	Binary Alignment and Map
Cacna1b	Calcium channel, voltage-dependent, N type, alpha 1B subunit
Ccna2	Cyclin A2
Cdc6	Cell division cycle 6
Cdh13	Cadherin 13
CEAS	Cis-Regulatory Element Annotation System
Celf5	CUGBP Elav-Like Family Member 5
Cenpf	Centromere protein F
Cntn2	Contactin 2
CO2	Carbon Dioxide
CRE	Cis Regulatory Element
DA	Dopaminergic
DMEM	Dulbecco's Modified Eagle Medium
Dpysl5	Dihydropyrimidinase-like 5
E13.5/15.5	Embryonic Day 13.5/15.5
ENCODE	Encyclopedia of DNA Elements
FB	Forebrain
FBS	Fetal Bovine Serum
FDR	False Discovery Rate
Foxa2	Forkhead Box A2
Gins1	GINS complex subunit 1 (*Psf1* homolog)
GO	Gene Ontology
GRCF	Genetics Core Research Facility
GWAS	Genome-Wide Association study
Hdac11	Histone deacetylase 11
Hmga2	High Mobility Group AT-Hook 2
Id2	Inhibitor Of DNA Binding 2
IGV	Integrative Genomics Viewer
Il33	Interleukin 33
Irx3	Iroquois Homeobox 3
LFC	Log Fold-Change
Lmx1b	LIM Homeobox Transcription Factor 1 Beta
MB	Midbrain
Mki67	Marker of Proliferation Ki-67
Nes	Nestin
Nova2	NOVA alternative splicing regulator 2
Nr4a2	Nuclear Receptor Subfamily 4 Group A, Member 2
Nrx1	Neurexin 1
Ntrk1	Neurotrophic receptor tyrosine kinase 1
OCR	Open Chromatin Region
Olig3	Oligodendrocyte transcription factor 3
PC(A)	Principal Component (Analysis)
pcHi-C	Promoter-Capture Hi-C
PD	Parkinson Disease
Pitx3	Paired-like homeodomain 3
Ptgds	Prostaglandin D2 synthase
(q)PCR	(Quantitative) Polymerase Chain Reaction
QC	Quality Control
RNA	Ribonucleic Acid
RPKM	Reads per kilobase of exon per million reads mapped
RT	Reverse Transcriptase
Scn1b	Sodium Voltage-Gated Channel Beta Subunit 1

scRNA-seq	Single Cell RNA sequencing
Slc6a3	Solute Carrier Family 6 Member 3
SN	Substantia Nigra
SNCA/Snca	Alpha-synuclein
SV40Tag	Simian Virus 40 T antigen
TH/Th	Tyrosine Hydroxylase
Tmem179	Transmembrane protein 179
ts	Temperature-Sensitive
TSS	Transcriptional Start Site
Unc13a	Unc-13 homolog A
vst	Variance Stabilizing Transformation

Supplementary Information

The online version contains supplementary material available at https://doi.org/10.1186/s12864-023-09398-y.

Additional file 1: Supplemental Table 1. RT-qPCR primers for testing expression of dopaminergic neuron markers. **Supplemental Figure 1.** ATAC-seq libraries are technically and biologically relevant. **Supplemental Figure 2.** ATAC-seq libraries are well correlated within and between temperature conditions. **Supplemental Figure 3.** Bulk RNA-seq Analysis. **Supplemental Figure 4.** In silico quality control metrics for all Promoter-capture Hi-C libraries with HiCUP.

Acknowledgements
The authors would like to acknowledge Ernest Arenas (Karolinska Institutet), for providing SN4741 cells, as well as the Johns Hopkins Genomics Core Research Facility (GCRF) and the WiCell Research Institute, for providing technical services.

Authors' contributions
New data was generated by S.A.M., P.W.H., W.D.L., E.W.L., and J.R; analyzed by R.J.B., S.A.M., P.W.H., N.B.B., W.D.L., and A.S.M. The manuscript was written by R.J.B., S.A.M., N.B.B., W.D.L., and A.S.M. Figures were created by R.J.B., S.A.M., and N.B.B. All authors reviewed and approved the manuscript.

Funding
This research, undertaken at Johns Hopkins University School of Medicine, was supported in part by awards from the National Institutes of Health (NS62972 and MH106522) to A.S.M., by T32 GM007814-40 to R.J.B. and N.B.B., and by the Canadian Institutes of Health Research (DFD-181599) to R.J.B.

Availability of data and materials
All data and analysis pipelines are available at https://github.com/rachelboyd. ATAC-sequencing, RNA-sequencing, single-cell RNA-sequencing, and promoter-capture Hi-C data is available at the Gene Expression Omnibus (GEO) under the series accession number GSE225084.

Declarations

Ethics approval and consent to participate
Not applicable.

Consent for publication
Not applicable.

Competing interests
The authors declare no competing interests.

Author details
[1]McKusick-Nathans Department of Genetic Medicine, Johns Hopkins University School of Medicine, Baltimore, MD 21205, USA. [2]Department of Medicine, Johns Hopkins University School of Medicine, Baltimore, MD 21287, USA.

Received: 27 January 2023 Accepted: 23 May 2023
Published online: 07 June 2023

References

1. Ormond KE, Mortlock DP, Scholes DT, Bombard Y, Brody LC, Faucett WA, et al. Human germline genome editing. Am J Hum Genet. 2017;101(2):167–76.
2. Barbosa DJ, Capela JP, de Lourdes BM, Carvalho F. In vitro models for neurotoxicology research. Toxicol Res. 2015;4(4):801–42.
3. Hirsch C, Schildknecht S. In vitro research reproducibility: keeping up high standards. Front Pharmacol. 2019;10:1484.
4. Fisher S, Grice EA, Vinton RM, Bessling SL, Urasaki A, Kawakami K, et al. Evaluating the biological relevance of putative enhancers using Tol2 transposon-mediated transgenesis in zebrafish. Nat Protoc. 2006;1(3):1297–305.
5. Gorkin DU, Lee D, Reed X, Fletez-Brant C, Bessling SL, Loftus SK, et al. Integration of ChIP-seq and machine learning reveals enhancers and a predictive regulatory sequence vocabulary in melanocytes. Genome Res. 2012;22(11):2290–301.
6. Shlyueva D, Stampfel G, Stark A. Transcriptional enhancers: from properties to genome-wide predictions. Nat Rev Genet. 2014;15(4):272–86.
7. Gasperini M, Findlay GM, McKenna A, Milbank JH, Lee C, Zhang MD, et al. CRISPR/Cas9-mediated scanning for regulatory elements required for HPRT1 expression via thousands of large, programmed genomic deletions. Am J Hum Genet. 2017;101(2):192–205.
8. Maurano MT, Humbert R, Rynes E, Thurman RE, Haugen E, Wang H, et al. Systematic localization of common disease-associated variation in regulatory DNA. Science (1979). 2012;337(6099):1190–5.
9. Kheradpour P, Ernst J, Melnikov A, Rogov P, Wang L, Zhang X, et al. Systematic dissection of regulatory motifs in 2000 predicted human enhancers using a massively parallel reporter assay. Genome Res. 2013;23(5):800–11.
10. Shim S, Kwan KY, Li M, Lefebvre V, Šestan N. Cis-regulatory control of corticospinal system development and evolution. Nature. 2012;486:74–9.
11. Schoenfelder S, Javierre BM, Furlan-Magaril M, Wingett SW, Fraser P. Promoter capture Hi-C: high-resolution, genome-wide profiling of promoter interactions. J Vis Exp. 2018;2018(136):e57320.
12. Schaub MA, Boyle AP, Kundaje A, Batzoglou S, Snyder M. Linking disease associations with regulatory information in the human genome. Genome Res. 2012;22(9):1748–59.
13. Ernst J, Kheradpour P, Mikkelsen TS, Shoresh N, Ward LD, Epstein CB, et al. Mapping and analysis of chromatin state dynamics in nine human cell types. Nature. 2011;473(7345):43–9.
14. Boyle EA, Li YI, Pritchard JK. An expanded view of complex traits: From polygenic to omnigenic. Cell. 2017;169(7):1177–86.
15. Lee D, Gorkin DU, Baker M, Strober BJ, Asoni AL, McCallion AS, et al. A method to predict the impact of regulatory variants from DNA sequence. Nat Genet. 2015;47(8):955–61.
16. Fearnley JM, Lees AJ. Ageing and Parkinson's disease: Substantia nigra regional selectivity. Brain. 1991;114:2283–301.
17. Marras C, Beck JC, Bower JH, Roberts E, Ritz B, Ross GW, et al. Prevalence of Parkinson's disease across North America. NPJ Parkinsons Dis. 2018;4(1):21.
18. Dorsey ER, Bloem BR. The Parkinson pandemic - a call to action. JAMA Neurol. 2018;75(1):9–10.
19. Ferrari E, Cardinale A, Picconi B, Gardoni F. From cell lines to pluripotent stem cells for modelling Parkinson's disease. J Neurosci Methods. 2020;340:108741.
20. Son JH, Chun HS, Joh TH, Cho S, Conti B, Lee JW. Neuroprotection and neuronal differentiation studies using substantia nigra dopaminergic cells derived from transgenic mouse embryos. J Neurosci. 1999;19(1):10.
21. Chang J, Le ZX, Yu H, Chen J. Downregulation of RTN1-C attenuates MPP+-induced neuronal injury through inhibition of mGluR5 pathway in SN4741 cells. Brain Res Bull. 2019;146:1–6.
22. Chen J, Li M, Zhou X, Xie A, Cai Z, Fu C, et al. Rotenone-induced neurodegeneration is enabled by a p38-Parkin-ROS signaling feedback loop. J Agric Food Chem. 2021;69(46):13942–52.
23. Guiney SJ, Adlard PA, Lei P, Mawal CH, Bush AI, Finkelstein DI, et al. Fibrillar α-synuclein toxicity depends on functional lysosomes. J Biol Chem. 2020;295(51):17497–513.
24. Chun HS, Gibson GE, Degiorgio LA, Zhang H, Kidd VJ, Son JH. Dopaminergic cell death induced by MPP+, oxidant and specific

neurotoxicants shares the common molecular mechanism. J Neurochem. 2001;76(4):1010–21.
25. Chun HS, Lee H, Son JH. Manganese induces endoplasmic reticulum (ER) stress and activates multiple caspases in nigral dopaminergic neuronal cells, SN4741. Neurosci Lett. 2001;316(1):5–8.
26. Zeng W, Zhang W, Lu F, Gao L, Gao G. Resveratrol attenuates MPP+-induced mitochondrial dysfunction and cell apoptosis via AKT/GSK-3β pathway in SN4741 cells. Neurosci Lett. 2017;637:50–6.
27. Cai Z, Zeng W, Tao K, Lu F, Gao G, Yang Q. Myricitrin alleviates MPP+-induced mitochondrial dysfunction in a DJ-1-dependent manner in SN4741 cells. Biochem Biophys Res Commun. 2015;458(2):227–33.
28. Mao K, Chen J, Yu H, Li H, Ren Y, Wu X, et al. Poly (ADP-ribose) polymerase 1 inhibition prevents neurodegeneration and promotes α-synuclein degradation via transcription factor EB-dependent autophagy in mutant α-synucleinA53T model of Parkinson's disease. Aging Cell. 2020;19(6):e13163.
29. Gui C, Ren Y, Chen J, Wu X, Mao K, Li H, et al. p38 MAPK-DRP1 signaling is involved in mitochondrial dysfunction and cell death in mutant A53T α-synuclein model of Parkinson's disease. Toxicol Appl Pharmacol. 2020;388:114874.
30. Dong Y, Xiong J, Ji L, Xue X. MiR-421 aggravates neurotoxicity and promotes cell death in Parkinson's disease models by directly targeting MEF2D. Neurochem Res. 2021;46(2):299–308.
31. Yoo MS, Chun HS, Son JJ, DeGiorgio LA, Kim DJ, Peng C, et al. Oxidative stress regulated genes in nigral dopaminergic neuronal cells: correlation with the known pathology in Parkinson's disease. Mol Brain Res. 2003;110(1):76–84.
32. Wang B, Cai Z, Lu F, Li C, Zhu X, Su L, et al. Destabilization of survival factor MEF2D mRNA by neurotoxin in models of Parkinson's disease. J Neurochem. 2014;130(5):720–8.
33. Dekker J, Rippe K, Dekker M, Kleckner N. Capturing chromosome conformation. Science (1979). 2002;295(5558):1306–11.
34. Lieberman-Aiden E, Van Berkum NL, Williams L, Imakaev M, Ragoczy T, Telling A, et al. Comprehensive mapping of long-range interactions reveals folding principles of the human genome. Science (1979). 2009;326(5950):289–93.
35. Mortazavi A, Williams BA, McCue K, Schaeffer L, Wold B. Mapping and quantifying mammalian transcriptomes by RNA-Seq. Nat Methods. 2008;5(7):621–8.
36. Buenrostro JD, Giresi PG, Zaba LC, Chang HY, Greenleaf WJ. Transposition of native chromatin for fast and sensitive epigenomic profiling of open chromatin, DNA-binding proteins and nucleosome position. Nat Methods. 2013;10(12):1213–8.
37. Nissim-Eliraz E, Zisman S, Schatz O, Ben-Arie N. Nato3 integrates with the Shh-Foxa2 transcriptional network regulating the differentiation of midbrain dopaminergic neurons. J Mol Neurosci. 2013;51:13–27.
38. Fishman-Jacob T, Reznichenko L, Youdim MBH, Mandel SA. A sporadic Parkinson disease model via silencing of the ubiquitin-proteasome/E3 ligase component SKP1A. J Biol Chem. 2009;284(47):32835–46.
39. Weihe E, Depboylu C, Schutz B, Schäfer MKH, Eiden LE. Three types of tyrosine hydroxylase-positive CNS neurons distinguished by dopa decarboxylase and VMAT2 co-expression. Cell Mol Neurobiol. 2006;26(4–6):659–78.
40. Jonakait GM, Markey KA, Goldstein M, Dreyfus CF, Black IB. Selective expression of high-affinity uptake of catecholamines by transiently catecholaminergic cells of the rat embryo: studies in vivo and in vitro. Dev Biol. 1985;108(1):6–17.
41. Cochard P, Goldstein M, Black IB. Ontogenetic appearance and disappearance of tyrosine hydroxylase and catecholamines in the rat embryo. Proc Natl Acad Sci U S A. 1978;75(6):2986–90.
42. Asmus SE, Parsons S, Landis SC. Developmental changes in the transmitter properties of sympathetic neurons that innervate the periosteum. J Neurosci. 2000;20(4):1495–504.
43. Ladd AN, Charlet-B. N, Cooper TA. The CELF family of RNA binding proteins is implicated in cell-specific and developmentally regulated alternative splicing. Mol Cell Biol. 2001;21(4):1285–96.
44. Nishino J, Kim I, Chada K, Morrison SJ. Hmga2 promotes neural stem cell self-renewal in young, but not old, mice by reducing p16Ink4a and p19Arf expression. Cell. 2008;135(2):227.
45. Park HJ, Hong M, Bronson RT, Israel MA, Frankel WN, Yun K. Elevated Id2 expression results in precocious neural stem cell depletion and abnormal brain development. Stem Cells. 2013;31(5):1010.
46. Dou Z, Son JE, Hui CC. Irx3 and Irx5 - Novel regulatory factors of postnatal hypothalamic neurogenesis. Front Neurosci. 2021;15:1447.
47. Reid CA, Leaw B, Richards KL, Richardson R, Wimmer V, Yu C, et al. Reduced dendritic arborization and hyperexcitability of pyramidal neurons in a Scn1b-based model of Dravet syndrome. Brain. 2014;137:1701–15.
48. Stark R, Brown GD. DiffBind: differential binding analysis of ChIP-Seq peak data. Bioconductor. 2011. Available online at: http://bioconductor.org/packages/release/bioc/html/DiffBind.html.
49. Li H, Liu Y, Gu Z, Li L, Liu Y, Wang L, et al. p38 MAPK-MK2 pathway regulates the heat-stress-induced accumulation of reactive oxygen species that mediates apoptotic cell death in glial cells. Oncol Lett. 2018;15(1):775.
50. McClymont SA, Hook PW, Soto AI, Reed X, Law WD, Kerans SJ, et al. Parkinson-associated SNCA enhancer variants revealed by open chromatin in mouse dopamine neurons. Am J Hum Genet. 2018;103(6):874–92.
51. Peng Y, Chu S, Yang Y, Zhang Z, Pang Z, Chen N. Neuroinflammatory In Vitro Cell Culture Models 796 and the Potential Applications for Neurological Disorders. Front Pharmacol. 2021;12:830.
52. Duval K, Grover H, Han LH, Mou Y, Pegoraro AF, Fredberg J, et al. Modeling physiological events 798 in 2D vs. 3D cell culture. Physiology. 2017;32(4):266–77.
53 Xie Z, Bailey A, Kuleshov M v., Clarke DJB, Evangelista JE, Jenkins SL, et al. Gene set knowledge 800 discovery with Enrichr. Curr Protoc. 2021;1(3):e90.
54. Chen EY, Tan CM, Kou Y, Duan Q, Wang Z, Meirelles G v., et al. Enrichr: interactive and 802 collaborative HTML5 gene list enrichment analysis tool. BMC Bioinformatics. 2013;14.
55. Kuleshov M v., Jones MR, Rouillard AD, Fernandez NF, Duan Q, Wang Z, et al. Enrichr: A 804 comprehensive gene set enrichment analysis web server 2016 update. Nucleic Acids Res. 805 2016;44(W1):W90–7.
56. Franzén O, Gan LM, Björkegren JLM. PanglaoDB: a web server for exploration of mouse and 807 human single-cell RNA sequencing data. Database. 2019;2019(1):46.
57. Zeng L, Zhang P, Shi L, Yamamoto V, Lu W, Wang K. Functional impacts of NRXN1 knockdown on 809 neurodevelopment in stem cell models. PLoS One. 2013;8(3).
58. Kaplan DR, Miller FD. Neurotrophin signal transduction in the nervous system. Curr Opin 811 Neurobiol. 2000;10(3):381–91.
59. Reddy-Alla S, Böhme MA, Reynolds E, Beis C, Grasskamp AT, Mampell MM, et al. Stable 813 positioning of Unc13 restricts synaptic vesicle fusion to defined release sites to promote 814 synchronous neurotransmission. Neuron. 2017;95(6):1350-1364.e12.
60. Storm R, Cholewa-Waclaw J, Reuter K, Bröhl D, Sieber M, Treier M, et al. The bHLH transcription 816 factor Olig3 marks the dorsal neuroepithelium of the hindbrain and is essential for the 817 development of brainstem nuclei. Development. 2009;136(2):295–305.
61. Sung HY, Chen WY, Huang HT, Wang CY, Chang S bin, Tzeng SF. Down-regulation of interleukin-33 819 expression in oligodendrocyte precursor cells impairs oligodendrocyte lineage progression. J 820 Neurochem. 2019;150(6):691–708.
62. Liu H, Hu Q, D'Ercole AJ, Ye P. Histone Deacetylase 11 regulates oligodendrocyte-specific gene 822 expression and cell development in OL-1 oligodendroglia cells. Glia. 2009;57(1):1.
63. Sakry D, Yigit H, Dimou L, Trotter J. Oligodendrocyte precursor cells synthesize neuromodulatory 824 factors. PLoS One. 2015;10(5).
64. Yam CH, Fung TK, Poon RYC. Cyclin A in cell cycle control and cancer. Cellular and Molecular Life 826 Sciences. 2002;59(8):1317–26.
65. Borlado LR, Méndez J. CDC6: from DNA replication to cell cycle checkpoints and oncogenesis. 828 Carcinogenesis. 2008;29(2):237–43.
66. Ma L, Zhao X, Zhu X. Mitosin/CENP-F in mitosis, transcriptional control, and differentiation. J 830 Biomed Sci. 2006;13(2):205–13.
67. Nagahama Y, Ueno M, Miyamoto S, Morii E, Minami T, Mochizuki N, et al. PSF1, a DNA 832 replication factor expressed widely in stem and progenitor cells, drives tumorigenic and 833 metastatic properties. Cancer Res. 2010;70(3):1215–24.
68. Szklarczyk D, Gable AL, Nastou KC, Lyon D, Kirsch R, Pyysalo S, et al. The STRING database in 835 2021: customizable protein-protein networks, and functional characterization of user-uploaded 836 gene/measurement sets. Nucleic Acids Res. 2021;49(D1):D605–12.

69. Choi KC, Kim SH, Ha JY, Kim ST, Son JH. A novel mTOR activating protein protects dopamine 838 neurons against oxidative stress by repressing autophagy related cell death. J Neurochem. 839 2010;112(2):366–76.
70. Bryja V, Čajánek L, Grahn A, Schulte G. Inhibition of endocytosis blocks Wnt signalling to β-841 catenin by promoting dishevelled degradation. Acta Physiologica. 2007;190(1):55–61.
71. Nalls MA, Blauwendraat C, Vallerga CL, Heilbron K, Bandres-Ciga S, Chang D, et al. Identification 843 of novel risk loci, causal insights, and heritable risk for Parkinson's disease: a meta-analysis of 844 genome-wide association studies. Lancet Neurol. 2019;18(12):1091–102.
72. Blauwendraat C, Nalls MA, Singleton AB, Blauwendraat C, Singleton AB, Nalls MA. The genetic 846 architecture of Parkinson's disease. Lancet Neurol. 2020;19:170–8.
73. Chang D, Nalls MA, Hallgrímsdóttir IB, Hunkapiller J, Brug M van der, Cai F, et al. A meta-analysis 848 of genome-wide association studies identifies 17 new Parkinson's disease risk loci. Nat Genet. 849 2017;49(10):1511–6.
74. Blauwendraat C, Heilbron K, Vallerga CL, Bandres-Ciga S, von Coelln R, Pihlstrøm L, et al. 851 Parkinson's disease age at onset genome-wide association study: Defining heritability, genetic 852 loci, and α-synuclein mechanisms. Movement Disorders. 2019;34(6):866–75.
75. Polymeropoulos MH, Lavedan C, Leroy E, Ide SE, Dehejia A, Dutra A, et al. Mutation in the α-854 synuclein gene identified in families with Parkinson's disease. Science (1979). 855 1997;276(5321):2045–7.
76. Singleton AB, Farrer M, Johnson J, Singleton A, Hague S, Kachergus J, et al. Alpha-synuclein locus 857 triplication causes Parkinson's disease. Science (1979). 2003;302(5646):841.
77. Ibáñez P, Bonnet AM, Débarges B, Lohmann E, Tison F, Pollak P, et al. Causal relation between 859 alpha-synuclein gene duplication and familial Parkinson's disease. The Lancet. 860 2004;364(9440):1169–71.
78. Taylor SC, Nadeau K, Abbasi M, Lachance C, Nguyen M, Fenrich J. The ultimate qPCR experiment: 862 Producing publication quality, reproducible data the first time. Trends Biotechnol. 863 2019;37(7):761–74.
79. Zheng GXY, Terry JM, Belgrader P, Ryvkin P, Bent ZW, Wilson R, et al. Massively parallel digital 865 transcriptional profiling of single cells. Nat Commun. 2017;8(1):1–12.
80. Butler A, Hoffman P, Smibert P, Papalexi E, Satija R. Integrating single-cell transcriptomic data 867 across different conditions, technologies, and species. Nat Biotechnol. 2018;36(5):411–20.
81. Corces MR, Trevino AE, Hamilton EG, Greenside PG, Sinnott-Armstrong NA, Vesuna S, et al. An 869 improved ATAC-seq protocol reduces background and enables interrogation of frozen tissues. 870 Nat Methods. 2017;14(10):959–62.
82. Andrews S, others. FastQC: a quality control tool for high throughput sequence data. 2010 872 [Internet]. https://www.bioinformatics.babraham.ac.uk/projects/fastqc/.. 2019. p. 873 https://www.bioinformatics.babraham.ac.uk/projects/.
83. Ewels P, Magnusson M, Lundin S, Käller M. MultiQC: summarize analysis results for multiple tools 875 and samples in a single report. Bioinformatics. 2016;32(19):3047–8.
84. Langmead B, Salzberg SL. Fast gapped-read alignment with Bowtie 2. Nat Methods. 877 2012;9(4):357.
85. Li H, Handsaker B, Wysoker A, Fennell T, Ruan J, Homer N, et al. The Sequence Alignment/Map 879 format and SAMtools. Bioinformatics. 2009;25(16):2078.
86. Zhang Y, Liu T, Meyer CA, Eeckhoute J, Johnson DS, Bernstein BE, et al. Model-based analysis of 881 ChIP-Seq (MACS). Genome Biol. 2008;9(9):1–9.
87. Amemiya HM, Kundaje A, Boyle AP. The ENCODE blacklist: Identification of problematic regions 883 of the genome. Sci Rep. 2019;9(1).
88. Dunham I, Kundaje A, Aldred SF, Collins PJ, Davis CA, Doyle F, et al. An integrated encyclopedia of 885 DNA elements in the human genome. Nature. 2012;489(7414):57–74.
89. Quinlan AR, Hall IM. BEDTools: a flexible suite of utilities for comparing genomic features. 887 Bioinformatics. 2010;26(6):841–2.
90. Ramírez F, Ryan DP, Grüning B, Bhardwaj V, Kilpert F, Richter AS, et al. deepTools2: A next 889 generation web server for deep-sequencing data analysis. Nucleic Acids Res. 890 2016;44(W1):W160–5.
91. Karolchik D, Hinricks AS, Furey TS, Roskin KM, Sugnet CW, Haussler D, et al. The UCSC Table 892 Browser data retrieval tool. Nucleic Acids Res. 2004;32(Database issue):D493.
92. Siepel A, Bejerano G, Pedersen JS, Hinrichs AS, Hou M, Rosenbloom K, et al. Evolutionarily 894 conserved elements in vertebrate, insect, worm, and yeast genomes. Genome Res. 895 2005;15(8):1034–50.
93. Shin H, Liu T, Manrai AK, Liu SX. CEAS: cis-regulatory element annotation system. Bioinformatics. 897 2009;25(19):2605–6.
94. Liu T, Ortiz JA, Taing L, Meyer CA, Lee B, Zhang Y, et al. Cistrome: An integrative platform for 899 transcriptional regulation studies. Genome Biol. 2011;12(8):1–10.
95. McLean CY, Bristor D, Hiller M, Clarke SL, Schaar BT, Lowe CB, et al. GREAT improves functional 901 interpretation of cis-regulatory regions. Nat Biotechnol. 2010;28(5):495–501.
96. Conway JR, Lex A, Gehlenborg N. UpSetR: an R package for the visualization of intersecting sets 903 and their properties. Bioinformatics. 2017;33(18):2938–40.
97. Kim D, Langmead B, Salzberg SL. HISAT: A fast spliced aligner with low memory requirements. Nat 905 Methods. 2015;12(4):357–60.
98. Gentleman RC, Carey VJ, Bates DM, Bolstad B, Dettling M, Dudoit S, et al. Bioconductor: Open 907 software development for computational biology and bioinformatics. Genome Biol. 2004;5(10).
99. Huber W, Carey VJ, Gentleman R, Anders S, Carlson M, Carvalho BS, et al. Orchestrating high-909 throughput genomic analysis with Bioconductor. Nat Methods. 2015;12(2):115–21.
100. Zhu A, Ibrahim JG, Love MI. Heavy-tailed prior distributions for sequence count data: removing the noise and preserving large differences. Bioinformatics. 2019;35(12):2084–92.
101. Liao Y, Smyth GK, Shi W. Sequence analysis featureCounts: an efficient general purpose program 913 for assigning sequence reads to genomic features. Bioinformatics. 2014;30(7):923–30.
102. Zhu A, Ibrahim JG, Love MI. Heavy-tailed prior distributions for sequence count data: removing 915 the noise and preserving large differences. Bioinformatics. 2019;35(12):2084–92.
103. Wickham H. ggplot2: Elegant Graphics for Data Analysis [Internet]. Springer-Verlag New York; 917 2016.
104. Belaghzal H, Dekker J, Gibcus JH. Hi-C 2.0: An optimized Hi-C procedure for high-resolution 919 genome-wide mapping of chromosome conformation. Methods. 2017;123:56–65.
105. Wingett S, Ewels P, Furlan-Magaril M, Nagano T, Schoenfelder S, Fraser P, et al. HiCUP: Pipeline for mapping and processing Hi-C data. F1000Res. 2015;4. https://doi.org/10.12688/f1000research.7334.1.
106. Cairns J, Freire-Pritchett P, Wingett SW, Várnai C, Dimond A, Plagnol V, et al. CHiCAGO: Robust detection of DNA looping interactions in Capture Hi-C data. Genome Biol. 2016;17(1):1–17.

Publisher's Note